


## Two-dimensional rare-earth Janus $2H$ -GdXY ( $X, Y = \text{Cl, Br, I}; X \neq Y$ ) monolayers: Bipolar ferromagnetic semiconductors with high Curie temperature and large valley polarization

Cunquan Li  and Yukai An \*

Key Laboratory of Display Materials and Photoelectric Devices, Ministry of Education, Tianjin Key Laboratory for Photoelectric Materials and Devices, National Demonstration Center for Experimental Function Materials Education, School of Material Science and Engineering, Tianjin University of Technology, Tianjin 300384, China

 (Received 3 November 2022; revised 8 February 2023; accepted 22 March 2023; published 29 March 2023)

Two-dimensional (2D) ferromagnetic semiconductors hold great interest due to their potential applications for nanoscale electronic devices. In this paper, the Janus  $2H$ -GdXY ( $X, Y = \text{Cl, Br, I}, X \neq Y$ ) monolayers with rare-earth element Gd ( $4f^7+5d^1$ ) are predicted by first-principles calculations. Small exfoliation energy of less than  $0.25 \text{ J/m}^2$  and excellent dynamical/thermal stabilities can be confirmed for the Janus  $2H$ -GdXY monolayers, which exhibit the bipolar magnetic semiconductor character with high Curie temperatures above 260 K and large spin-orbit coupling effect, and can be further transformed into the half-semiconductor phase under proper tensile strains (5–6%). In addition, in-plane magnetic anisotropy can be observed in the  $2H$ -GdICl and  $2H$ -GdIBr monolayers. On the contrary, the  $2H$ -GdBrCl monolayer exhibits perpendicular magnetic anisotropy character, which originates from the competition between Gd- $p/d$  and halogen atom- $p$  orbitals. Calculated valley optical actions of the Janus  $2H$ -GdXY monolayers exhibit distinguished valley-selective circular dichroisms, which is expected to realize the special valley excitation by polarized light. Spontaneously, valley-Zeeman effect in the valance band for the Janus  $2H$ -GdXY monolayers induces a giant valley splitting of 60–120 meV, which is also robust against various external biaxial strains. A tunable valley degree of freedom in Janus  $2H$ -GdXY systems is very necessary for encoding and processing information.

DOI: [10.1103/PhysRevB.107.115428](https://doi.org/10.1103/PhysRevB.107.115428)

### I. INTRODUCTION

Two-dimensional (2D) materials show increasing interest owing to their broad application prospects in nanoscale electronic devices. It has been proved by the Mermin-Wagner theorem that 2D magnetic ordering can be prohibited due to thermal fluctuations [1]. As a breakthrough development, intrinsic ferromagnetic (FM) ordering was experimentally discovered in the  $\text{CrI}_3$  [2] and  $\text{VI}_3$  [3] monolayers, which exhibit Curie temperatures ( $T_C$ ) of 45 K and 49 K, respectively. These studies attract much attention and further stimulate looking for 2D magnetic materials at the nanoscale. Significant progress has been made with 2D materials with magnetic ordering, while the rare intrinsic semiconducting ferromagnetism and low  $T_C$  limit their potential applications in spintronic devices [4–6]. The  $T_C$  of 2D materials can be effectively enhanced by applying the charge carrier doping [7], biaxial strain [8], and external electric fields [9], etc. However, these methods are still not ideal solutions for the practical applications in spintronics.

Transition metal dichalcogenide (TMD) chloride monolayers with a hexagonal structure have a pair of nonequivalent energy valleys at the Dirac points of the Brillouin zone, which can be excited using left- or right-handed light and attract a great deal of attention. The valley, which indicates the maximum of a valence band or minimum of a conduction

band, is an additional degree of freedom of carriers besides the charge and spin. The two inequivalent valleys constitute a binary index for low-energy carriers and this degree of freedom can be encoded and manipulated as an information carrier in valleytronics [10]. Inspired by the analysis above, searching for intrinsic ferro-valley (FM materials with spontaneous valley polarization) [11] materials with high  $T_C$  and large valley polarization are necessary for candidates of valleytronics. To realize this, it is vital to choose a system with special electrons and orbitals. Recently, rare-earth element-based systems, especially for the Gd element, have become a hot topic of research. In fact, as early as 1965, Mee and Corbett [12] synthesized the block  $\text{GdI}_2$  with a van der Waals structure. Very recently, a  $\text{GdI}_2$  monolayer with high  $T_C$  of 241 K and sizable magnetic anisotropy energy (MAE) was predicted by Wang *et al.* [13], and its large valley polarization (149 meV) and robustness to external biaxial strain were investigated by Cheng *et al.* [14]. Immediately after,  $\text{GdX}_2$  ( $X = \text{I, F, Cl, Br}$ ) monolayers [15–17] were further predicted, especially that the  $\text{GdCl}_2$  monolayer shows high  $T_C$  of about 224 K and large perpendicular magnetic anisotropy (PMA) character. Experimentally, Janus (special types of materials which have two faces at the nanoscale) TMD monolayers have been synthesized successfully in special conditions [18,19]. And, based on DFT calculations, some magnetic Janus monolayers, such as  $\text{FeClBr}$  [20],  $\text{MnSSe}$  [21],  $\text{Cr}_2\text{X}_3\text{S}_3$  ( $X = \text{Br, I}$ ) monolayers [22], etc. have been predicted. Due to the super-/direct-exchange interactions and spin-orbit coupling (SOC) in these 2D magnetic Janus systems, an intrinsic valley

\*ykan@tjut.edu.cn

polarization can be observed in both valence and conduction bands. Furthermore, for the Janus  $2H$ -GdClF monolayer with FM ordering, it is noted that the tunable valley polarization can be observed and driven by external biaxial strains [23]. In light of these key factors about systems with the Gd element mentioned above, the Janus  $2H$ -GdXY monolayers can be expected as a ferrovalley material with large valley polarization and are very likely to be synthesized by surface replacement technology [18].

In this paper, the stability, valley polarization, and magnetic anisotropy of Janus  $2H$ -GdXY monolayers are systematically studied by DFT calculations. All Janus  $2H$ -GdXY monolayers show FM semiconductor characteristics with high  $T_C$  beyond 260 K. Interestingly, only the  $2H$ -GdBrCl monolayer possesses PMA behavior, while the  $2H$ -GdICl and  $2H$ -GdIBr monolayers exhibit the in-plane magnetic anisotropy (IMA) character. The competition between Gd atom- $p/d$  orbitals and halogen atom- $p$  orbitals can result in a transition of easy axis direction from the [001] to [100] plane for the Janus  $2H$ -GdXY monolayers. A spontaneous and robust valley polarization is observed, which can be effectively adjusted by the external biaxial strains.

## II. COMPUTATIONAL DETAILS

All density functional theory (DFT) calculations are performed using the projected augmented wave [24,25] approach as implemented in the VIENNA AB INITIO SIMULATION PACKAGE (VASP) [26,27]. Considering the exchange and correlation functional interactions, the Perdew-Burke-Ernzerhof (PBE) within generalized gradient approximation is applied [28]. The van der Waals correction is considered for the bulk GdXY using the Grimme (DFT-D3) method [29]. The plane wave cut-off energy is set to 500 eV and a vacuum space of 18 Å is applied along the  $z$ -axis [001] direction to avoid interactions between adjacent layers. The crystal structure of the Janus  $2H$ -GdXY monolayers is completely relaxed until a force of less than 0.01 eV/Å per atom and an energy difference of less than  $10^{-6}$  eV between two convergence steps is observed. The Brillouin zone is sampled using converged  $\Gamma$ -centered  $k$  meshes with a density of 144  $k$ -points ( $12 \times 12 \times 1$ ) for structural relaxation and 576  $k$  points ( $24 \times 24 \times 1$ ) for the electronic calculations [30]. The electron configurations including  $5s^25p^64f^75d^16s^2$  for Gd [31],  $4s^24p^5$  for Br,  $3s^23p^5$  for Cl, and  $5s^25p^5$  for I atoms are considered. The SOC effect is included in the calculations to investigate electronic, magnetic, and valley-related properties of the Janus  $2H$ -GdXY monolayers. The rotationally invariant local spin density approximation + Hubbard ( $U$ ) method is employed to treat the strongly correlated corrections to the Gd  $4f$  electrons [32] and the corresponding on-site  $U$ /exchange interaction  $J$  parameters is set at 9.20 eV/1.20 eV [13,33]. The phonon dispersion spectrum of the Janus  $2H$ -GdXY monolayers are obtained by the PHONOPY code [34,35] using a  $2 \times 2 \times 1$  supercell. *Ab initio* molecular dynamic (AIMD) simulations [36] adopt the moles-volume-temperature (NVT) ensemble [37] based on the Nosé-Hoothermostat [38] controlled the temperature of systems at 300 K with a total of 8.0 ps at 2.0 fs per time step. The VASPKIT code is used to process some of the VASP data [39]. The  $T_C$  of the Janus  $2H$ -GdXY monolayers are estimated by

using the Monte Carlo simulation package MCSOLVER [40] based on the Wolff algorithm. The Berry curvature and optical properties are calculated based on Fukui's method [41] by VASPBERRY code, which was developed by Kim *et al.* [42].

## III. RESULTS AND DISCUSSION

Figure 1(a) displays the crystal structure of the Janus  $2H$ -GdXY monolayers. Clearly, the loss of reflection symmetry of Gd atom reduces the symmetry of the systems. The optimized lattice constants for the  $2H$ -GdBrCl,  $2H$ -GdICl, and  $2H$ -GdIBr monolayers are 3.835, 3.96, and 4.019 Å, respectively. The FM and antiferromagnetic (AFM) ordering of crystal structures for the Janus  $2H$ -GdXY monolayers is shown in Figs. 1(b) and 1(c). The FM stability energies ( $\Delta E = E_{AFM} - E_{FM}$ ) between the FM and AFM ordering for the  $2H$ -GdBrCl,  $2H$ -GdICl, and  $2H$ -GdIBr monolayers are 165.2, 154.9, and 152.2 meV, respectively, strongly suggesting the existence of FM coupling among three systems. Figure S1 of the Supplemental Material (SM) [43] shows the spin density images of the Janus  $2H$ -GdXY monolayers. One can see that the magnetic moments are mainly contributed by the Gd and Cl (Br) atoms for the Janus  $2H$ -GdICl ( $2H$ -GdIBr) monolayers and by all Gd, Cl, and Br atoms for the Janus  $2H$ -GdBrCl monolayer, suggesting that the valence electrons tend to gather around the Cl (Br) atom with stronger electronegativity. To prove the stability of Janus  $2H$ -GdXY monolayers, the calculations of phonon dispersion and AIMD simulation are carried out. As shown in Figs. 1(d)–1(f), the phonon dispersions exhibit a positive value in the whole Brillouin zone, strongly suggesting the dynamical stability for the Janus  $2H$ -GdXY monolayers. In addition, with time evolution, the small fluctuations (about  $\pm 1$  eV) of free energy, the total magnetic moment is kept at about  $128.0 \mu_B$  and the original configuration does not show large distortion, implying a good thermal stability of the Janus  $2H$ -GdXY monolayers (Fig. S2(a)–S2(c) of the SM [43]). To estimate the possibility of mechanical exfoliation, the exfoliation energy of the Janus  $2H$ -GdXY monolayers is calculated in four-layer slab models with AB stacking [44] (Fig. S3(a) of the SM [43]) from their layered bulk crystals. Considering the small value of separation distance, the exfoliation process is performed with the fixed atomic positions. As shown in Figs. S3(b)–S3(d) of the SM [43], the increase of separation distance ( $d - d_0$ ) leads to an obvious increase in the energy differences  $\Delta E = E_d - E_{d_0}$ , which converge to 0.232, 0.243, and 0.239 J/m<sup>2</sup>, respectively, for the Janus  $2H$ -GdBrCl,  $2H$ -GdICl, and  $2H$ -GdIBr monolayers, respectively. These cleavage energies are remarkably lower than the measured value (0.36 J/m<sup>2</sup>) for graphite [45], which can be further confirmed by the variation of cleavage strength (the first-order derivative of cleavage energy). This means that the Janus  $2H$ -GdXY monolayers are easy to exfoliate experimentally. The band structures of the Janus  $2H$ -GdXY monolayers without considering SOC are shown in Figs. 2(a)–2(c). The energies at the K and K' valleys are equal, suggesting that the valley splitting does not appear without considering SOC. The typical bipolar magnetic semiconductor character [BMS: the valence and conduction bands possess opposite spin polarization when approaching the Fermi level ( $E_F$ )] [46] with an indirect band gap can be

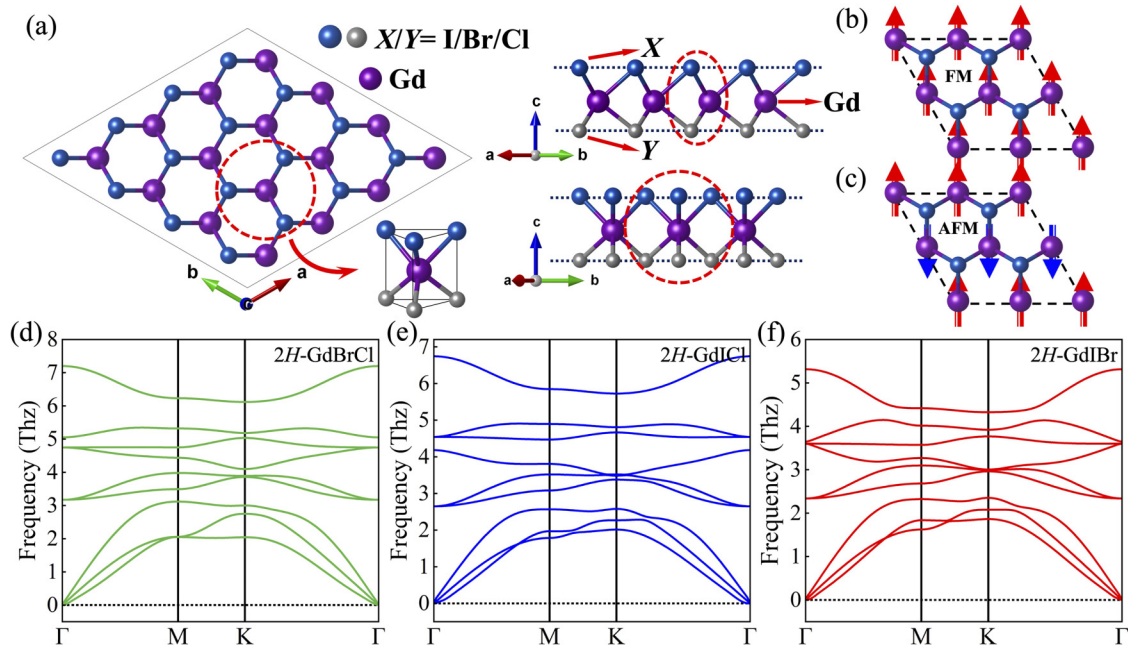


FIG. 1. (a) Top/side views of the Janus  $2H\text{-GdXY}$  monolayers and the coordination environment of the Gd atom. The unit cell is marked by the red lines. The (b) FM and (c) AFM states of crystal structures; red (blue) arrow shows the direction of spin-up (spin-down). The phonon dispersion of the Janus (d)  $2H\text{-GdBrCl}$ , (e)  $2H\text{-GdICl}$ , and (f)  $2H\text{-GdIBr}$  monolayers.

observed, where the valence band maximum (VBM) located at the  $\Gamma$  point and the conduction band minimum (CBM) located at the  $M$  point have the opposite spin polarization orientation. The band gaps for the Janus  $2H\text{-GdBrCl}$ ,  $2H\text{-GdICl}$ , and  $2H\text{-GdIBr}$  monolayers are about 480.1, 513.1, and 476.2 meV, respectively. Figures S4(a)-S4(c) of the SM [43] show the corresponding orbital-resolved

density of states (DOS) curves of three systems. One can see that the VBM and CBM of the Janus  $2H\text{-GdXY}$  monolayers are dominated by  $d$  orbitals of Gd atoms. The narrow and high distribution of DOS for Gd- $f$  orbitals are around 3 eV above the  $E_F$ . As a result, the  $5d$  electrons are fully spin polarized in the vicinity of the  $E_F$  and the induced moments of  $4f$  electrons can effectively align around

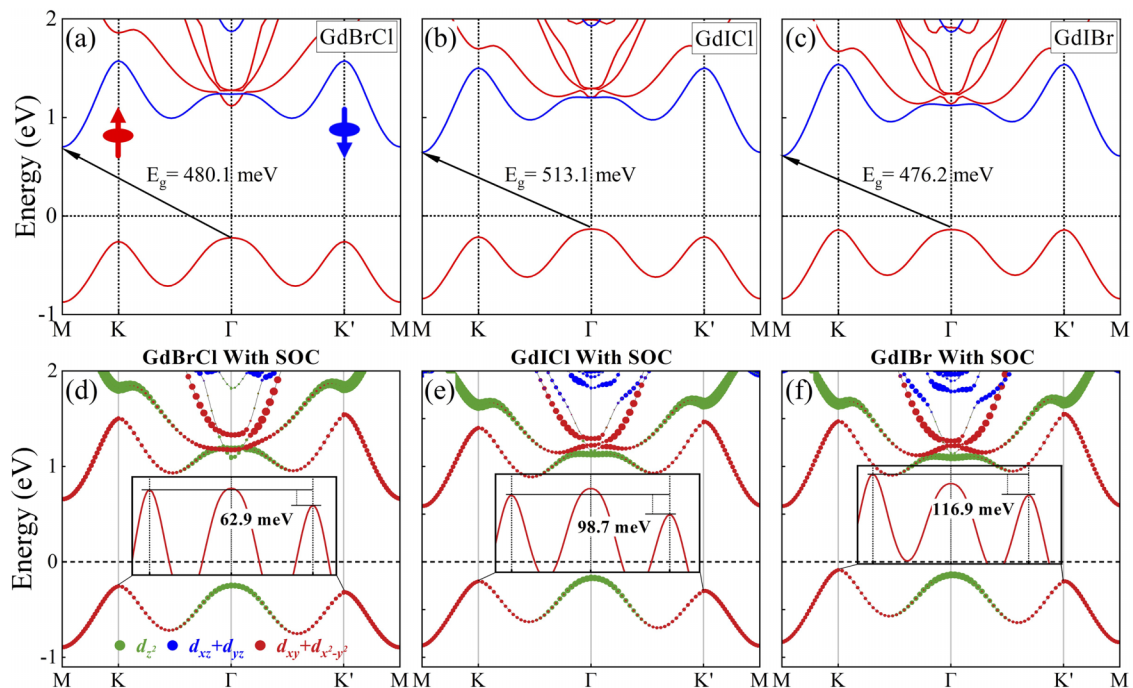


FIG. 2. The projected PBE band structures for the Janus  $2H\text{-GdXY}$  monolayers (a)–(c) without and (d)–(f) with considering SOC. The Fermi level is set to zero.



the polarized  $5d$  electrons by a cooperative mechanism, resulting in intrinsic large magnetic moments [47]. On the contrary, the DOS of halogen atoms comes from their  $p$  orbitals, and is far away from the  $E_F$ , suggesting a weak hybridization between the  $p$  orbitals of halogen atoms and  $4f$  orbitals of Gd atoms. Generally, we consider that two magnetic exchange interaction mechanisms, namely, the Gd-Gd direct-exchange interaction and the Gd- $X(Y)$ -Gd superexchange interaction ( $X, Y$  represent the halogen atoms), are responsible for the FM ordering in the Janus  $2H$ -GdXY monolayers, especially that the superexchange FM (AFM) interaction occurs when the bond angle between cation and anion ions is close to  $90^\circ$  ( $180^\circ$ ) by the Goodenough-Kanamori-Anderson rule [48–50]. It is noted that the bond angles of Gd- $X(Y)$ -Gd in the three systems almost reach  $90^\circ$ , namely, Cl:  $86.645^\circ$  (Br:  $82.018^\circ$ ) in the  $2H$ -GdBrCl, I:  $78.962^\circ$  (Cl:  $89.159^\circ$ ) in the  $2H$ -GdICl, and I:  $80.18^\circ$  (Br:  $85.70^\circ$ ) in the  $2H$ -GdIBr, strongly suggesting the existence of superexchange FM interaction between the Gd  $5d$  and  $X(Y)$ - $4p$  orbitals. In addition, the nearest Gd-Gd distance in the Janus  $2H$ -GdXY monolayers is larger than  $3.8 \text{ \AA}$ , which is much larger than the radii of  $d$ - or  $f$ -orbital carrying magnetic moments. Thus, based on the above analysis, the superexchange interaction is the dominant mechanism for the FM coupling between the nearest-neighboring Gd cations mediated by  $X/Y$  anions in Janus  $2H$ -GdXY monolayers, which comes from the  $p$ - $d$  hybridization between the  $X/Y$ - $4p$  and Gd- $5d$  orbitals.

Figures 2(d)–2(f) display the projected band structures of the Janus  $2H$ -GdXY monolayers with considering SOC. Clearly, the K ( $K'$ ) valley still exists (same as the spin polarization), but the energies at the K and  $K'$  valleys are not equal and the degeneracy of the valley is broken. The energy at the K valley is higher than that at the  $K'$  valley in the VBM, resulting in a large valley polarization of 62.9, 98.7, and 116.9 meV for the  $2H$ -GdBrCl,  $2H$ -GdICl, and  $2H$ -GdIBr monolayers, respectively. Also, the K and  $K'$  valleys in the valence band mainly come from in-plane  $d_{xy}/d_{x^2-y^2}$  orbitals and  $\Gamma$  point is contributed by the out-of-plane  $d_{z^2}$  orbital. Based on the above analysis, the electronic structures, valley, and magnetic properties are expected to strongly depend on the occupation of in-plane atomic orbitals for the Janus  $2H$ -GdXY monolayers.

Figure 3(a) shows the biaxial strain dependencies on the FM stability energy  $\Delta E$  for the Janus  $2H$ -GdXY monolayers. Clearly, the FM stability energy  $\Delta E$  gradually decreases with increasing the strain ( $\epsilon$ ) from  $-8\%$  to  $8\%$ , suggesting that applying in-plane biaxial strain can well adjust the FM exchange interaction of studies systems. One can see from Figs. 3(b)–3(d), and Fig. S5 of the SM [43] that with the increase of tensile strain, the band edge difference of CMB at the  $M$  and  $\Gamma$  points between the spin- $\alpha$  (spin-up) and spin- $\beta$  (spin-down) electrons can be expressed as  $\Delta E_{\text{CBM}-\Gamma-M} = E_{\text{CBM}-\Gamma-\alpha} - E_{\text{CBM}-\Gamma-\beta}$ . For the unstrained Janus  $2H$ -GdBrCl,  $2H$ -GdICl and  $2H$ -GdIBr monolayers,  $\Delta E_{\text{CBM}-\Gamma-M} = 0.4135, 0.5545, \text{ and } 0.5286 \text{ eV}$ , respectively. Clearly, the  $E_g-\alpha$  and  $E_g$  show a monotonous decrease trend, while the  $E_g-\beta$  increases monotonously. When the tensile strain (about  $5$ – $6\%$ ) is applied, the  $\Delta E_{\text{CBM}-\Gamma-M}$  is up to  $0 \text{ eV}$ , indicating a transition from BMS to half semiconductor (HSC) [51] character for the Janus  $2H$ -GdXY monolayers, namely, both VBM and CBM are occupied by the same spin

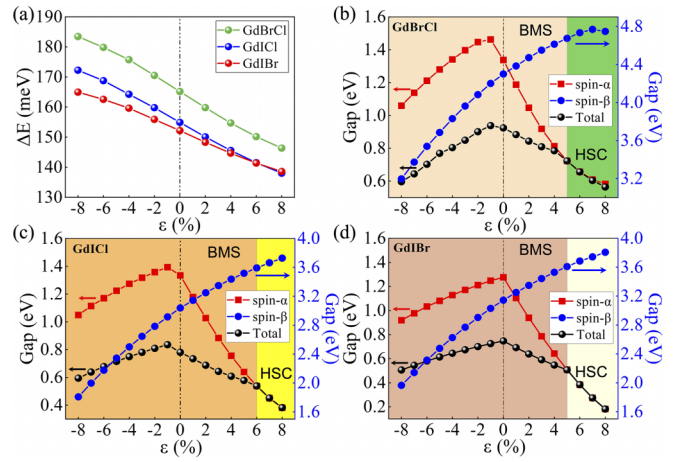


FIG. 3. (a) The biaxial strain dependencies on the ferromagnetic stability energy  $\Delta E$  for the Janus  $2H$ -GdXY monolayers. The biaxial strain dependencies on  $E_g-\alpha$ ,  $E_g-\beta$ , and  $E_g$  for the (b)  $2H$ -GdBrCl, (c)  $2H$ -GdICl, and (d)  $2H$ -GdIBr monolayers.

direction elections (spin  $\alpha$ ). As the tensile strain increases continuously, the Janus  $2H$ -GdXY monolayers still keep HSC character. Interestingly, this transition from BMS to HSC character does not appear under compressive strain due to the occupation of spin- $\alpha$  electrons. Under the biaxial strains varying from  $-8\%$  to  $0\%$ , the Janus  $2H$ -GdXY monolayers still maintain BMS character due to the occupation of spin- $\beta$  electrons in the CBM, which shows a monotonous decrease with strain for the spin-down band gap  $E_g-\beta$ .

Magnetic anisotropy (MA) is one key factor to realize the long-range magnetic ordering in 2D materials, which directly correlates with the thermal stability of magnetic data storage. The MA can be scaled by MAE, which is expressed as  $\text{MAE} = E_{[001]} - E_{[100]}$ , where  $E_{[001]}$  and  $E_{[100]}$  are the energies of system when the magnetic moments are along the out-of-plane  $[001]$  axis and the in-plane  $[100]$  axis, respectively. The MAE values for the Janus  $2H$ -GdICl and  $2H$ -GdIBr monolayers are  $0.289$  and  $0.419 \text{ meV}$ , respectively, showing the IMA character. Moreover, the MAE value of  $-0.029 \text{ meV}$  implies a PMA character for the Janus  $2H$ -GdBrCl monolayer. Figure 4(a) shows the biaxial strain dependencies on total MAE of Janus  $2H$ -GdXY monolayers, which exhibits a monotonous increase behavior with increasing the strain from  $-8\%$  to  $8\%$ . The biaxial strain dependencies on atomic-resolved MAEs are shown in Figs. 4(b)–4(d). The halogen  $X$  ( $Y$ ) atom in the Janus  $2H$ -GdXY monolayers always keeps the IMA behavior at the whole strain ranges. Moreover, the MAE from the Gd atom increases monotonously with the increase of tensile or compressive strains, and a transition from the PMA to IMA behavior can be observed. Figures 5(a)–5(c) show the MAE of the Janus  $2H$ -GdXY monolayers along  $xy$ ,  $xz$ , and  $yz$  planes. Clearly, for all Janus  $2H$ -GdXY monolayers, the MAE exhibits a strong dependence of the magnetization direction along the  $xz$  and  $yz$  planes. Further, the MAE as a function of angle  $\theta$  can be expressed as [52]

$$\text{MAE}(\theta) = K_1 \sin^2 \theta + K_2 \sin^4 \theta \quad (1)$$

and

$$\text{MAE}(\theta) = K_3 \cos^2 \theta + K_4 \cos^4 \theta, \quad (2)$$

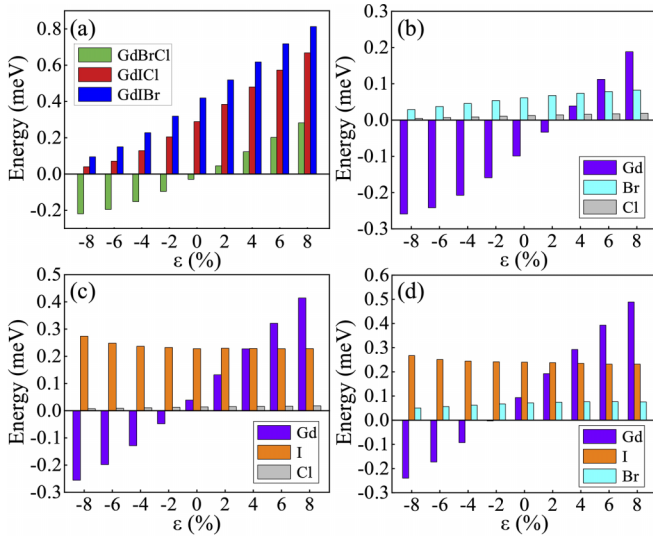


FIG. 4. The (a) total MAE and (b)–(d) atoms-resolved MAE for the Janus 2H-GdXY monolayers.

where  $K_1$  ( $K_2$ ) and  $K_3$  ( $K_4$ ) are the anisotropy constants. The angle theta  $\theta$  refers to an arbitrary azimuthal angle  $\theta$  [ $0^\circ$ ,  $180^\circ$ ]. It is clear that the MAE is independent of the angle  $\theta_{xy}$  ( $xy$  plane). For the 2H-GdBrCl monolayer, the best fitting data ( $K_1 > 0$  and  $K_1 \gg K_2$ ) of MAE dependence on  $\theta$  show a magnetization direction along out-of-plane axis while, for the 2H-GdICl and 2H-GdIBr monolayer, both  $K_3$  and  $K_4$  are positive, revealing that the MAE of the two systems prefer a single easy axis. The strong magnetic anisotropy of the three systems is also confirmed by the distribution of MAE on the whole spaces (Fig. 5(d) and Fig. S6 of the SM [43]). The calculated orbital-resolved MAE based on the spin-orbit matrix element differences [53] is used to investigate its origins and can be expressed as

$$\text{MAE} = \xi^2 \sum_{o,u} \frac{|\langle \psi_o | \hat{L}_z | \psi_u \rangle|^2 - |\langle \psi_o | \hat{L}_x | \psi_u \rangle|^2}{E_u - E_o}, \quad (3)$$

where  $E_o$  ( $E_u$ ) represents the energy of the occupied (unoccupied) state and the  $\xi$  is the SOC constant. As is shown in Figs. 5(e) and 5(f), for the Janus 2H-GdXY monolayers, the negative MAE is contributed by the Gd- $p$  orbital. On the contrary, the sizable positive MAE comes from the contribution of Gd- $d$  and I- $p$  orbitals. Other Gd- $f$  and Br/Cl- $p$  orbitals only give an almost negligible contribution to the MAE. Therefore, the difference in the total MAE for the Janus 2H-GdXY monolayers is a competitive result of the Gd- $d$ -/ $p$  and  $X$  ( $Y$ )- $p$  orbitals. As the  $X$  ( $Y$ ) changes from the I to Br (Cl) atom, the net value of total MAE of  $p$  orbitals of  $X$  ( $Y$ ) atoms decrease, resulting in out-of-plane MA for the Janus 2H-GdBrCl monolayer.

$T_C$  is an important indicator for the potential applications of magnetic devices. To evaluate the  $T_C$  of the Janus 2H-GdXY monolayers, the Metropolis Monte Carlo simulations are carried out based on the Heisenberg model. Following the previous work [17], we only considered the nearest Gd-Gd magnetic interaction. The spin Hamiltonian can be described

with the following formulas:

$$H = -J \sum_{i,j} \vec{S}_i \cdot \vec{S}_j - D(S_i^z)^2, \quad (4)$$

where  $J$  represents the magnetic exchange parameter,  $S$  is the spin vector, and  $D$  is an anisotropy energy parameter,

$$E_{\text{FM}} = E_0 - 6J|S|^2 - D|S|^2, \quad (5)$$

$$E_{\text{AFM}} = E_0 + 2J|S|^2 - D|S|^2, \quad (6)$$

where the  $E_{\text{FM}}$  and  $E_{\text{AFM}}$  represent the total energy of systems with FM and AFM ordering. The magnetic exchange parameter  $J$  with considering nearest-neighbor coordination can be expressed using the following formula:

$$J = \frac{E_{\text{AFM}} - E_{\text{FM}}}{8|S|^2}. \quad (7)$$

The calculated  $J$  values for the Janus 2H-GdBrCl, 2H-GdICl, and 2H-GdIBr monolayers are 1.29, 1.21, and 1.188 meV, respectively, strongly suggesting the existence of FM ordering around the nearest-neighbor Gd atom. Figures 6(a) and 6(b) show the magnetic moments ( $M_{\text{Gd}}$ ) and specific heat for the Janus 2H-GdXY monolayers as functions of temperature. The calculated  $T_C$  values are about 281, 264, and 260 K, respectively, for the Janus 2H-GdBrCl, 2H-GdICl, and 2H-GdIBr monolayers, which are obviously higher than those observed in the  $\text{CrI}_3$  (45 K) [2] and  $\text{VI}_3$  (49 K) [3] monolayers.

Figure 7(a) shows the valley optical transitions with  $\sigma^+$  ( $\sigma^-$ ) circular polarizations at the K ( $K'$ ) valleys, which describes the intrinsic transport arising from the electronic structures of unequal K ( $K'$ ) valley. Further, the carriers of K and  $K'$  valleys can be selectively excited by the valley-selective circular dichroism with different chiral lights, which has been proved in the nonmagnetic  $\text{MoS}_2$  system [54]. Inspired by this, for investigating corresponding optical properties, the degree of circular polarization is calculated by

$$\eta(k) = \frac{|p_+^{V,C}(k)|^2 - |p_-^{V,C}(k)|^2}{|p_+^{V,C}(k)|^2 + |p_-^{V,C}(k)|^2}, \quad (8)$$

where  $p_{\pm}^{V,C}(k) = p_x^{V,C}(k) \pm ip_y^{V,C}(k)$  and the matrix element is given by  $p_{\pm}^{V,C}(k) = \langle \psi_j^V | \hat{p}_{\pm} | \psi_k^C \rangle$ . The  $k$ -resolved quantity distinguishes left ( $\sigma^+$ ) and right ( $\sigma^-$ ) circularly polarized light between the valence and conduction bands with band index V and C, respectively. Figure 7(b) shows the circular polarization  $\eta(k)$  of optical transition for the Janus 2H-GdBrCl monolayer over the first Brillouin zone. It can be found that  $\eta(k)$  is nearly +1 (−1) at the K and  $K'$  valleys, indicating that left ( $\sigma^+$ ) and right ( $\sigma^-$ ) circularly polarized light can only excite the corresponding K and  $K'$  valleys, respectively. Meanwhile, the Berry curvature of the matrix element  $p_{\pm}^{V,C}(k)$  is given by [55,56]

$$\Omega_n(k) = -\frac{\hbar^2}{2m} \sum_{V \neq C} \frac{\eta^{V,C}(k)[|p_+^{V,C}(k)|^2 + |p_-^{V,C}(k)|^2]}{[E_C(k) - E_V(k)]^2}. \quad (9)$$

Clearly, the transformation property of  $\eta^{V,C}(k)$  follows that of  $\Omega_n(k)$ , which can be confirmed by our following work.

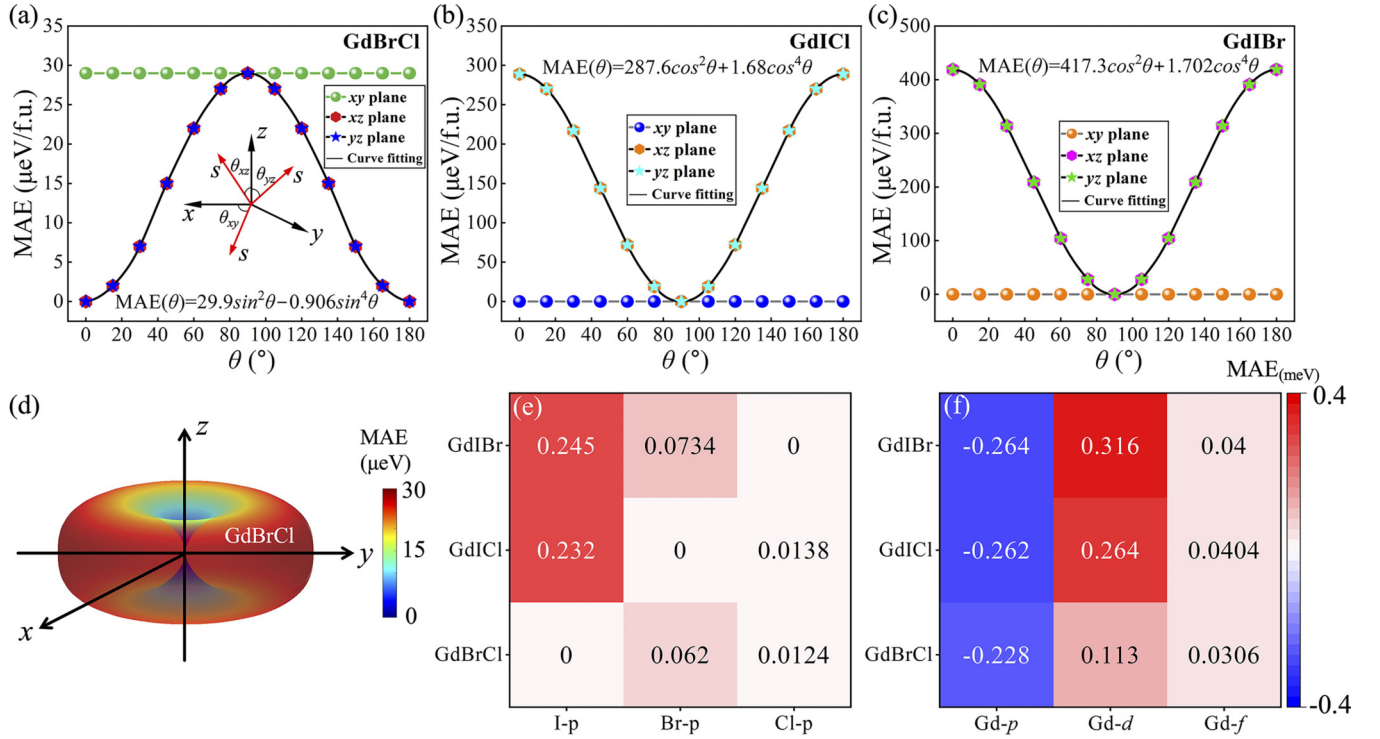


FIG. 5. MAE of the (a)–(c) Janus  $2H$ -GdXY monolayers along  $xy$ ,  $xz$  and  $yz$  planes and (d) over the whole space for the  $2H$ -GdBrCl monolayer. The contributions of (e) Br/I/Cl- $p$  orbitals and (e) Gd- $p$ , - $d$ , - $f$  orbitals to MAE for the Janus  $2H$ -GdXY monolayers.

After clarifying the spontaneous valley polarization in Janus  $2H$ -GdXY monolayers, we finally consider their Berry curvatures along the out-of-plane direction  $[001]$  to describe their electronic transport properties, which is critical for quantum Hall effects. The Berry curvature of Janus  $2H$ -GdXY monolayers can be defined as [57–59]

$$\Omega_n(k) = \nabla \times C_n(k), \quad (10)$$

$$C_n(k) = i\langle u_n(k) | \nabla_k | u_n(k) \rangle, \quad (11)$$

where  $n$  is the band index and  $u_n(k)$  is the Bloch wave functions. For the Janus  $2H$ -GdXY monolayers, all valence electrons below the  $E_F$  are considered during the calculation of the Berry curvature. The Berry curvatures of the Janus  $2H$ -GdXY monolayers over the whole 2D Brillouin zone and along the high-symmetry lines are shown in Figs. 8(a)–8(d). It is clear that the intensity of Berry curvatures at the  $K'$  valley is larger than that at the  $K$  valley, accompanied by the opposite signs. Interestingly, two valleys in the valence band are not only distinguishable in terms of energy, but also

can be distinguished by the value of their Berry curvature. Figure 8(e) shows the schematic diagram of anomalous valley Hall effects under external electric fields  $E$ . One can see that when the Janus  $2H$ -GdXY monolayers are magnetized along the  $z$  direction, the spin-down holes from the  $K'$  valley move to the left-hand side of the sample and are further accumulated on the boundary under the external electric field  $E$ . Conversely, when the magnetic field direction is altered along the  $-z$  direction, the spin-up holes from the  $K$  valley move to the right-hand side of the sample and are accumulated on another boundary due to the opposite Berry curvature under the same electric field  $E$ . Therefore, the valley degree of freedom of carriers in the Janus  $2H$ -GdXY monolayers can be selectively manipulated by the electric measurements, which is significant for designing the valleytronic devices. An external biaxial strain is applied on the Janus  $2H$ -GdXY monolayers

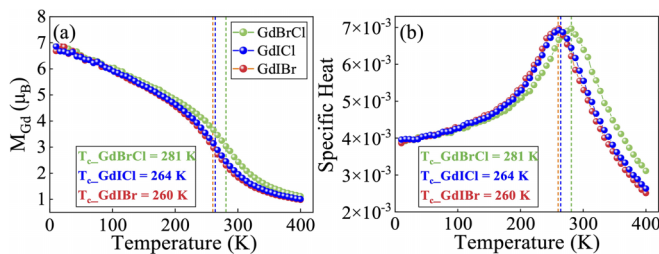


FIG. 6. (a) The magnetic moments ( $M_{\text{Gd}}$ ) and (b) specific heat for the Janus  $2H$ -GdXY monolayers as functions of temperature.

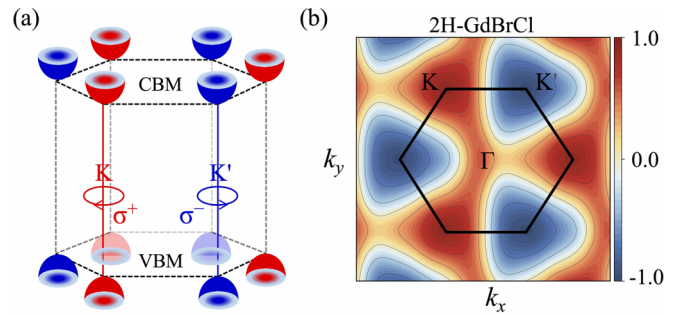


FIG. 7. (a) The valley optical transitions with  $\sigma^+$  ( $\sigma^-$ ) circular polarizations at the  $K$  ( $K'$ ) valleys. (b) The circular polarization  $\eta(k)$  of optical transition for the Janus  $2H$ -GdBrCl monolayer over the first Brillouin zone.



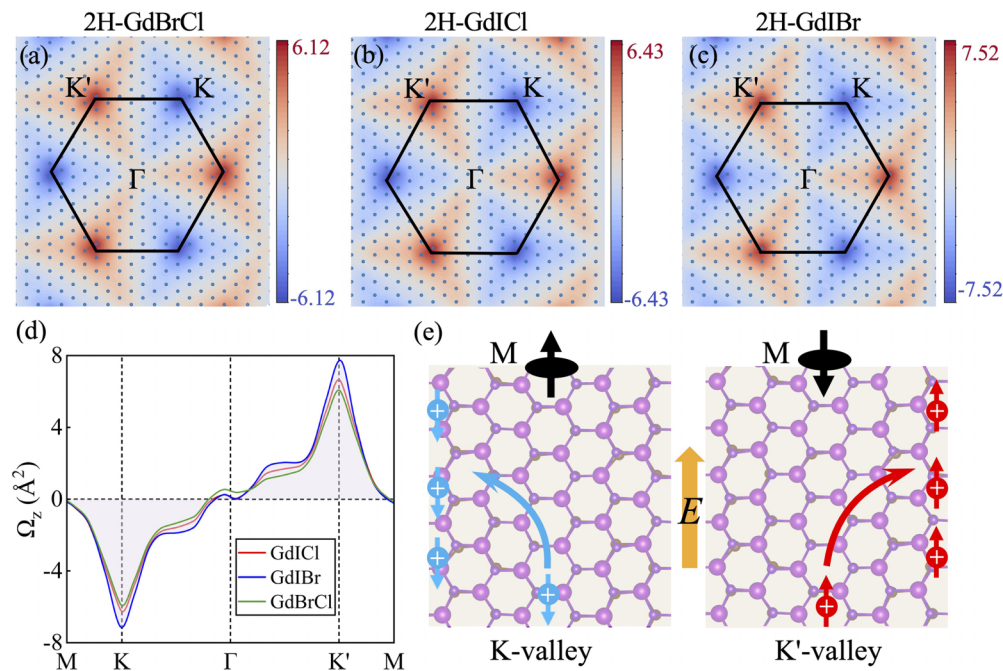


FIG. 8. (a)–(c) Contour map of Berry curvatures as well as (d) Berry curvatures along the high-symmetry points for the Janus  $2H$ -GdXY monolayers. (e) Schematic diagram of anomalous valley Hall effects under external electric fields  $E$ . The red and blue arrows represent the spin-up and spin-down holes.

to investigate the robustness of the ferro-valley characters. Figures S7(a) and S7(b) of the SM [43] show the variation of valley splitting of the Janus  $2H$ -GdXY monolayers as a function of biaxial strains from  $-8\%$  to  $8\%$ . Obviously, as the tensile (compressive) strains increase from  $0\%$  to  $8\%$  ( $-8\%$ ), the valley splitting shows a monotonical increase (decrease) in behavior. The valley polarization values of Janus  $2H$ -GdBrCl,  $2H$ -GdCl and  $2H$ -GdIBr monolayers reaches 113.1, 142.7 and 158.8 meV at tensile strain of  $8\%$ , respectively. Conversely, under a compressive strain of  $8\%$ , valley polarization values decrease to 16.8 and 36.7 meV for the  $2H$ -GdCl and  $2H$ -GdIBr monolayers, respectively, implying a robust valley polarization against the biaxial strains. Interestingly, the energies of the K and  $K'$  valleys reverse for the  $2H$ -GdBrCl monolayer, accompanied by a valley splitting of  $-20.8$  meV. Therefore, the Janus  $2H$ -GdXY monolayers are excellent ferro-valley materials with large and tunable valley splitting, which is necessary to readily access and manipulate valleys for memory and logic applications.

#### IV. CONCLUSIONS

In summary, by first-principles calculations, the electronic structure, valley polarization, and MA of the Janus  $2H$ -GdXY

monolayers were systematical investigated, which exhibit FM semiconductor character with excellent dynamic/thermal stability. The estimated  $T_C$  based on the Monte Carlo simulations are 284, 264, and 260 K for the  $2H$ -GdBrCl,  $2H$ -GdCl, and  $2H$ -GdIBr monolayers, respectively. The magnetic easy axis direction of  $2H$ -GdCl and  $2H$ -GdIBr monolayers is along the in-plane direction. However, a transition from IMA to PMA occurs for the  $2H$ -GdBrCl monolayer, which can be attributed due to the competition between the contributions of Gd- $p/-d$  and  $X(Y)$ - $p$  orbitals to MAE. In addition, the valley polarization of Janus  $2H$ -GdXY monolayers are robust against the external strains. Moreover, due to the breaking of time-reversal and inversion symmetry, nonzero out-of-plane Berry curvature is observed for the Janus  $2H$ -GdXY monolayers, which makes it possible to realize the anomalous valley Hall effect. Overall, our paper provides a platform for the development of spin/valleytronic devices.

#### ACKNOWLEDGMENTS

This work was supported by the Natural Science Foundation of Tianjin City (Grant No. 20JCYBJC16540).

- [1] N. D. Mermin and H. Wagner, *Phys. Rev. Lett.* **17**, 1133 (1966).  
 [2] B. Huang, G. Clark, E. Navarro-Moratalla, D. R. Klein, R. Cheng, K. L. Seyler, D. Zhong, E. Schmidgall, M. A. McGuire, and D. H. Cobden, *Nature (London)* **546**, 270 (2017).  
 [3] T. Kong, K. Stolze, E. I. Timmons, J. Tao, D. Ni, S. Guo, Z. Yang, R. Prozorov, and R. J. Cava, *Adv. Mater.* **31**, 1808074 (2019).  
 [4] J.-F. Dayen, S. J. Ray, O. Karis, I. J. Vera-Marun, and M. V. Kamalakar, *Appl. Phys. Rev.* **7**, 011303 (2020).  
 [5] S. Chen, C. Huang, H. Sun, J. Ding, P. Jena, and E. Kan, *J. Phys. Chem. C* **123**, 17987 (2019).  
 [6] I. Žutić, J. Fabian, and S. D. Sarma, *Rev. Mod. Phys.* **76**, 323 (2004).

- [7] S. Jiang, L. Li, Z. Wang, K. F. Mak, and J. Shan, *Nat. Nanotechnol.* **13**, 549 (2018).
- [8] H. Y. Lv, W. J. Lu, X. Luo, X. B. Zhu, and Y. P. Sun, *Phys. Rev. B* **99**, 134416 (2019).
- [9] H. Li, S. Ruan, and Y. Zeng, *Adv. Mater.* **31**, 1900065 (2019).
- [10] K. F. Mak, D. Xiao, and J. Shan, *Nature Photon.* **12**, 451 (2018).
- [11] W.-Y. Tong, S.-J. Gong, X. Wan, and C.-G. Duan, *Nat. Commun.* **7**, 13612 (2016).
- [12] J. E. Mee and J. D. Corbett, *Inorg. Chem.* **4**, 88 (1965).
- [13] B. Wang, X. Zhang, Y. Zhang, S. Yuan, Y. Guo, S. Dong, and J. Wang, *Mater. Horiz.* **7**, 1623 (2020).
- [14] H.-X. Cheng, J. Zhou, W. Ji, Y.-N. Zhang, and Y.-P. Feng, *Phys. Rev. B* **103**, 125121 (2021).
- [15] K. Sheng, H.-K. Yuan, and Z.-Y. Wang, *Phys. Chem. Chem. Phys.* **24**, 3865 (2022).
- [16] F. Ding, S. Ji, S. Li, L. Wang, H. Wu, Z. Hu, F. Li, and Y. Pu, *Phys. Status Solidi* **258**, 2100356 (2021).
- [17] W. Liu, J. Tong, L. Deng, B. Yang, G. Xie, G. Qin, F. Tian, and X. Zhang, *Mater. Today Phys.* **21**, 100514 (2021).
- [18] A.-Y. Lu, H. Zhu, J. Xiao, C.-P. Chuu, Y. Han, M.-H. Chiu, C.-C. Cheng, C.-W. Yang, K.-H. Wei, and Y. Yang, *Nat. Nanotechnol.* **12**, 744 (2017).
- [19] J. Zhang, S. Jia, I. Kholmanov, L. Dong, D. Er, W. Chen, H. Guo, Z. Jin, V. B. Shenoy, and L. Shi, *ACS Nano* **11**, 8192 (2017).
- [20] R. Li, J. Jiang, X. Shi, W. Mi, and H. Bai, *ACS Appl. Mater. Interfaces* **13**, 38897 (2021).
- [21] Y. Chen, Q. Fan, Y. Liu, and G. Yao, *Phys. Rev. B* **105**, 195410 (2022).
- [22] D. Wu, Z. Zhuo, H. Lv, and X. Wu, *J. Phys. Chem. Lett.* **12**, 2905 (2021).
- [23] S.-D. Guo, X.-S. Guo, X.-X. Cai, and B.-G. Liu, *Phys. Chem. Chem. Phys.* **24**, 715 (2022).
- [24] G. Kresse and D. Joubert, *Phys. Rev. B* **59**, 1758 (1999).
- [25] P. E. Blöchl, *Phys. Rev. B* **50**, 17953 (1994).
- [26] G. Kresse and J. Furthmüller, *Phys. Rev. B* **54**, 11169 (1996).
- [27] G. Kresse and J. Furthmüller, *Comput. Mater. Sci.* **6**, 15 (1996).
- [28] J. P. Perdew, K. Burke, and M. Ernzerhof, *Phys. Rev. Lett.* **77**, 3865 (1996).
- [29] S. Grimme, J. Antony, S. Ehrlich, and H. Krieg, *J. Chem. Phys.* **132**, 154104 (2010).
- [30] H. J. Monkhorst and J. D. Pack, *Phys. Rev. B* **13**, 5188 (1976).
- [31] H. You, Y. Zhang, J. Chen, N. Ding, M. An, L. Miao, and S. Dong, *Phys. Rev. B* **103**, L161408 (2021).
- [32] P. Larson, W. R. L. Lambrecht, A. Chantis, and M. van Schilfgaarde, *Phys. Rev. B* **75**, 045114 (2007).
- [33] H. Jamnezhad and M. Jafari, *J. Comput. Electron.* **16**, 272 (2017).
- [34] A. Togo and I. Tanaka, *Scr. Mater.* **108**, 1 (2015).
- [35] X. Gonze and C. Lee, *Phys. Rev. B* **55**, 10355 (1997).
- [36] D. Bucher, L. C. T. Pierce, J. A. McCammon, and P. R. L. Markwick, *J. Chem. Theory Comput.* **7**, 890 (2011).
- [37] S. Nosé, *Mol. Phys.* **52**, 255 (1984).
- [38] S. Nosé, *J. Chem. Phys.* **81**, 511 (1984).
- [39] V. Wang, N. Xu, J.-C. Liu, G. Tang, and W.-T. Geng, *Comput. Phys. Commun.* **267**, 108033 (2021).
- [40] L. Liu, X. Ren, J. Xie, B. Cheng, W. Liu, T. An, H. Qin, and J. Hu, *Appl. Surf. Sci.* **480**, 300 (2019).
- [41] T. Fukui, Y. Hatsugai, and H. Suzuki, *J. Phys. Soc. Jpn.* **74**, 1674 (2005).
- [42] S.-W. Kim, H.-J. Kim, S. Cheon, and T.-H. Kim, *Phys. Rev. Lett.* **128**, 046401 (2022).
- [43] See Supplemental Material at <http://link.aps.org/supplemental/10.1103/PhysRevB.107.115428> for more simulation results on the structural, magnetic, and electronic properties of the Janus 2H-GdXY monolayer.
- [44] S. Li, W. Jiang, Y. Hou, F. Zheng, X. Shao, and P. Zhang, *J. Appl. Phys.* **130**, 043902 (2021).
- [45] R. Zacharia, H. Ulbricht, and T. Hertel, *Phys. Rev. B* **69**, 155406 (2004).
- [46] X. Li, X. Wu, Z. Li, J. Yang, and J. Hou, *Nanoscale* **4**, 5680 (2012).
- [47] L. E. Roy, Doctoral dissertation, Texas A&M University, 2006.
- [48] J. B. Goodenough, *Phys. Rev.* **100**, 564 (1955).
- [49] J. Kanamori, *J. Appl. Phys.* **31**, S14 (1960).
- [50] P. W. Anderson, *Phys. Rev.* **115**, 2 (1959).
- [51] Z. Guan, N. Luo, S. Ni, and S. Hu, *Mater. Adv.* **1**, 244 (2020).
- [52] Y. Z. Abdullahi, Z. D. Vatansever, F. Ersan, U. Akinci, O. U. Akturk, and E. Akturk, *Phys. Chem. Chem. Phys.* **23**, 6107 (2021).
- [53] X. Wang, R. Wu, D.-s. Wang, and A. J. Freeman, *Phys. Rev. B* **54**, 61 (1996).
- [54] W. Feng, Y. Yao, W. Zhu, J. Zhou, W. Yao, and D. Xiao, *Phys. Rev. B* **86**, 165108 (2012).
- [55] W. Yao, D. Xiao, and Q. Niu, *Phys. Rev. B* **77**, 235406 (2008).
- [56] M.-C. Chang and Q. Niu, *Phys. Rev. B* **53**, 7010 (1996).
- [57] D. Xiao, M.-C. Chang, and Q. Niu, *Rev. Mod. Phys.* **82**, 1959 (2010).
- [58] A. Kormányos, V. Zólyomi, V. I. Fal'ko, and G. Burkard, *Phys. Rev. B* **98**, 035408 (2018).
- [59] X. Liu, A. P. Pyatakov, and W. Ren, *Phys. Rev. Lett.* **125**, 247601 (2020).